Thermodynamic modeling of melt addition to peridotite: implications for the refertilization of the non-cratonic continental mantle lithosphere

Juliette Pin, Lydéric France, Sarah Lambart, Laurie Reisberg

Thermodynamic modeling of melt addition to peridotite: implications for the refertilization of the non-cratonic continental mantle lithosphere

Submitted to Chemical Geology

Juliette Pin[1,2*], Lydéric France[1,3], Sarah Lambart[4], Laurie Reisberg[1]

1. Université de Lorraine, CNRS, CRPG, F-54000 Nancy, France

2. Univ. Brest, CNRS, IUEM, UMR 6538, Laboratoire Géosciences Océan, Place Copernic, 29280 Plouzané, France

3. Institut Universitaire de France (IUF)

4. Department of Geology and Geophysics, University of Utah, Salt Lake City, UT, United States

***corresponding author:**

juliette.pin@univ-brest.fr

Keywords: continental mantle lithosphere; refertilization; mixing model; peridotites; pHMELTS; harzburgites; lherzolites.

Abstract:

In a classic model of evolution of the non-cratonic continental mantle lithosphere, harzburgites represent the refractory (< 5% clinopyroxene) residues of high degrees of partial melting of fertile mantle, while lherzolites (> 5% clinopyroxene) represent residues of lesser degrees of partial melting. However, partial melting is not the only process that could explain the peridotite compositional variability that ranges from fertile (> 2 wt.% Al_2O_3, <45 wt.% MgO) to refractory (< 2 wt.% Al_2O_3, > 45 wt.% MgO). In the refertilization process, harzburgite is a refractory protolith (potentially previously formed by partial melting of a fertile mantle) that undergoes reactive percolation of silicate melts derived from the underlying asthenosphere, resulting in the crystallization of a new generation of minerals (mostly clinopyroxene). A simple but critical first step towards understanding the refertilization process is to examine how modal and major element compositions evolve as melts are added to peridotites. Here we use a thermodynamically-constrained two-component mixing model to independently evaluate the roles of five different parameters: pressure, temperature, redox conditions, and compositions of the initial peridotite and the added basaltic melt (hereafter referred to P-T-fO_2-Xπ-Xmelt), during melt addition. We compare the results with observed suites of peridotites. The main observations are as follows: (1) the produced model is consistent with the global peridotite database, and (2) T, fO_2 and small variations of pressure have almost no impact on the evolution of the system. In contrast, the mineralogy of the percolated harzburgite has a substantial effect on the variation of the modal proportions. The parameter with the most significant impact is Xmelt, which is directly linked to the geodynamic context and melting conditions. This parameter directly controls the refertilization reaction and so, the phase proportions and the bulk-rock composition. Elements that partition preferentially in the melt phase (e.g., Na) display depletions in natural assemblages that are stronger than those predicted from the simple mixing model, consistent with the fact that the natural process occurs in an open system, and that reactive percolation likely results in incompatible element enrichment in the associated melt. Our results corroborate the suggestion that most of the spectrum of

compositional variability observed in lithospheric mantle peridotites can be explained by the impregnation of primitive silicate melt in refractory harzburgites.

1. Introduction

The subcontinental lithospheric mantle (SCLM) is petrologically and geochemically heterogeneous (Allègre & Turcotte, 1986; Hofmann, 1997; Stracke et al., 2005; Griffin et al., 2009; Bodinier & Godard, 2014; Pearson et al., 2014). This lithospheric domain is documented by xenoliths in alkali basalts and kimberlites and by orogenic peridotite massifs. In non-cratonic regions, the SCLM has on average a lherzolitic bulk composition (> 5% clinopyroxene; Griffin et al., 1999). Lherzolites are fertile peridotites, and are aluminum-rich (> 2 wt.% Al_2O_3) and magnesium-poor (< 45 wt.% MgO). Pyroxenites, dunites and, to a greater extent, harzburgites (< 5% clinopyroxene) are also common SCLM lithologies. Harzburgites are aluminum-poor (< 2 wt.% Al_2O_3) and magnesium-rich (> 45 wt.% MgO). The genetic relationships between these rock types have been the subject of much debate in the last decades (e.g., Frey and Prinz, 1978; Kelemen et al., 1992; Le Roux et al., 2007). In addition to potential preexisting compositional variability, the spectrum of natural peridotite compositions can be mostly explained by the combination of two end-member processes (**Fig. 1**): partial melting and refertilization (see reviews by Simon et al., 2008; Bodinier and Godard, 2014; Pearson et al., 2014; Warren, 2016). The partial melting model implies that harzburgites and clinopyroxene-poor lherzolites are formed by variable degrees of partial melting of fertile lherzolites (e.g., Dick et al., 1984; Frey et al., 1985; McKenzie and Bickle, 1988; McKenzie and O'Nions, 1991; Hellebrand et al., 2001). The refertilization model implies that lherzolites are secondary (refertilized) lithologies formed from the interaction between a refractory, lithospheric mantle (mostly harzburgitic) with silicate melts derived from the underlying asthenosphere (e.g., Van der Wal and Bodinier, 1996; Garrido and Bodinier, 1999; Muntener and Piccardo, 2003; Pilet et al, 2005, 2008, 2011) or, more locally, from a secondary melting event of the lithosphere (e.g., Chazot et al., 1996; Rampone et al., 2020). As used in this contribution, the term "refertilization" will refer to the process of modal transformation of harzburgite from the addition of, and/or interaction with silicate melt in the non-cratonic mantle. This can produce clinopyroxene-enriched harzburgite, lherzolite, or other types of peridotite depending on

77 the percolating melt composition. We do not consider the full range of metasomatic processes and
78 agents that often result in the enrichment of incompatible trace elements and modification of isotopic
79 compositions in peridotites. Nevertheless, we recognize that refertilization and metasomatism
80 represent a continuum of processes and the distinction between them can be ambiguous. We also do
81 not consider processes of metamorphic segregation (e.g., Tilhac et al., 2021) that can contribute to
82 local sharp changes of modal proportions.

83 Support for the refertilization model is provided by petrographic, geochemical and structural
84 observations. Geochemical evidence comprises variations of trace and major elements in bulk
85 compositions and minerals (e.g., Elthon, 1992; Hellebrand et al., 2002; Le Roux et al., 2007; Soustelle
86 et al., 2009; Mundl et al., 2015; Gu et al., 2016), while structural observations include lherzolite
87 foliations and websterite layering that cross-cut harzburgite deformation (Le Roux et al., 2008).
88 Additionally, the presence of intergranular pyroxenes and spinels, often associated with sulfides
89 (Bodinier & Godard, 2014; Lorand and Luguet, 2016) has been interpreted as secondary phase
90 crystallization from liquid percolation. Al_2O_3 content in the bulk-rock is very frequently used as a
91 proxy for peridotite fertility, though MgO and CaO contents, Yb and Lu concentrations, olivine Fo#
92 (=MgO/(MgO+FeO)*100, in mol.) and spinel Cr# (=Cr_2O_3/(Cr2O3+Al_2O_3)*100, in mol.) are also
93 often used (e.g., Gao et al., 2002; Handler et al., 2003; Wu et al., 2006; Armytage et al., 2014; Byerly
94 and Lassiter, 2012). Most fertility proxy correlations can be interpreted by both partial melting and
95 refertilization processes, but there are exceptions. Elthon (1992) showed that the linear relationship
96 between Na_2O and MgO observed in abyssal peridotites was inconsistent with partial melting, but
97 could be explained by refertilization. In addition, variations of major, minor and trace elements
98 through the harzburgite-lherzolite contacts in the Lherz massif indicate that the lherzolites were
99 formed through a refertilization process (Le Roux et al., 2007). The refertilization mechanism also
100 provides a key to understanding the paradoxical association of light rare earth element (LREE)
101 enrichment with depleted harzburgite often observed in mantle xenoliths and in tectonically-emplaced
102 peridotites (e.g., Frey and Prinz, 1978; McDonough and Frey, 1989; Godard et al., 1995; Le Roux et
103 al., 2007; Tilhac et al., 2021). Finally, radiogenic isotope signatures, such as those of Hf, Nd, Sr and

Os (e.g., Saal et al., 2001; Müntener et al., 2004; Le Roux et al., 2009, 2016; Lawley et al., 2020; Borghini et al., 2021; Reisberg, 2021), have often been attributed to the effects of refertilization, though this effect may be indirect, reflecting radiogenic ingrowth following ancient enrichment. For instance, the negative correlation of $^{87}Sr/^{86}Sr$ with Al_2O_3 and the positive correlation of $^{143}Nd/^{144}Nd$ with Al_2O_3 observed in Pyrenean peridotites (Downes et al., 1991; Bodinier & Godard, 2003) probably result from refertilization, with the most likely scenario being radiogenic decay following ancient enrichment in incompatible elements by a percolating melt with a depleted (MORB-like) isotopic composition (Le Roux et al., 2007). Similarly, frequently observed positive correlations between $^{187}Os/^{188}Os$ and Al_2O_3 in lithospheric peridotites may reflect radiogenic ingrowth after refertilization occurring soon after ancient melting events (Reisberg, 2021).

Formation of lherzolites by refertilization of depleted harzburgite during percolation of a silicate melt is frequently proposed to explain the composition of peridotite suites, notably in the Lherz massif (Pyrénées, France), type-locality of lherzolites (Le Roux et al., 2007), but also in numerous other worldwide occurrences including the Western Gneiss Region of Norway (Beyer, 2006), abyssal peridotites (Elthon, 1992; Seyler et al., 2007), or peridotite suites from the Kaapvaal craton (Simon et al., 2007) among other examples. Given the Os isotope evidence that large-scale refertilization can be temporally associated with the melting event that led to harzburgite depletion, refertilization is sometimes viewed as an integral part of the melting process, and has been described as "autometasomatism" (Rudnick and Walker, 2008). When melt circulation in the mantle is more channelized, cumulative pyroxenites may form (Bodinier et al., 2008; France et al., 2015; Tilhac et al., 2016; Borghini et al., 2020; Dai et al., 2021); such pyroxenites are among the most fertile mantle lithologies, and could thus be important components in any potential subsequent partial melting episode (e.g., Lambart et al., 2013; France et al., 2015).

An improved knowledge of refertilization of lithospheric peridotites is critical to understanding how the continental lithosphere developed its current composition. In this contribution, we investigate the influence of various parameters such as pressure, temperature, and redox conditions, as well as the chemical composition of the initial peridotite and percolating melt on the chemical and modal

composition of the resulting solid phase, using a thermodynamically based mixing model. Our model considers lithospheric processes related to the percolation of melts formed in the major melting regime, and does not explore the related processes with strongly silica-undersaturated liquid that form near the solidus under oxidized conditions (e.g., on the carbonated peridotite solidus). A similar approach (thermodynamic model of peridotite impregnation by a silicate melt) has been adopted by Lambart et al. (2012) and Shaw et al. (2018). Lambart et al. (2012) produced a simplified model of impregnation of a peridotite by a pyroxenite-derived melt at constant P and T, resulting in the generation of various peridotitic and pyroxenitic lithologies with systematic production of clinopyroxene. Shaw et al. (2018) were able to produce wehrlites by addition of orthopyroxene-undersaturated mafic alkaline magma to orthopyroxene bearing peridotite, followed by isobaric equilibration. While our approach is not entirely new, the goal of this paper is to determine the minimal number of parameters required to explain the SCLM compositional variability, as well as to confirm if the current understanding of the refertilization process is thermodynamically viable. The main goal of this paper is to determine whether a simple mixing model can reproduce both the bulk composition and the modal proportions of non-cratonic SCLM peridotites. Although simple (and therefore incomplete), our model is consistent with a global database of orogenic peridotites (Bodinier and Godard, 2014).

2. Approach

In this section, we reproduce the two end-member models: (1) mixing at constant P-T-fO_2 conditions during which a fixed mass of melt is progressively added to a refractory peridotite, and (2) partial melting of a fertile lherzolite.

2.1. pHMELTS and Adiabat-1ph

In this study, we aim to test if the refertilization of a refractory peridotite by a silicate melt can explain the range of modal proportions observed in global non-cratonic lithospheric peridotites. We used the thermodynamic model pHMELTS (Asimow et al., 2004) and the adiabat-1ph front end (Smith & Asimow, 2005) to model the effects of magma impregnation in peridotites at constant pressure,

157 temperature and oxygen fugacity. The pHMELTS model calculates equilibrium assemblages in
158 peridotitic systems by minimizing the Gibbs energy of the system from constraints on bulk
159 composition, temperature, pressure or volume, enthalpy or entropy, and/or oxygen fugacity. The
160 pHMELTS routine is part of the MELTS group of algorithms (Ghiorso & Sack, 1995). These
161 algorithms are used to model mantle melting and magma crystallization, and also allow for melt-rock
162 impregnation models. We use the pHMELTS software as it is suitable for pressures comprised
163 between 1 and 3 GPa (Hirschmann et al., 1998), relevant for the non-cratonic SCLM.

164 The interface adiabat-1ph (Smith & Asimow, 2005) allows the automation of pHMELTS calculations.
165 It is used to calculate equilibrium assemblages along a thermodynamic path. In particular, we used the
166 'Adiabat assimilate' option of the front-end to simulate the impregnation process as it allows us to add
167 a fixed mass of melt after each calculation stage at constant P and T conditions. The output
168 parameters (e.g., phase proportions and compositions) are calculated at each step along the
169 thermodynamic path after equilibrium conditions are achieved.

170 The use of pHMELTS is subject to certain constraints due to the proven limits of the software:

171 - The subsolidus routines do not handle K_2O well if feldspar is not present (Asimow &
172 Ghiorso, 1998). We therefore did not consider potassium.
173 - The incorporation of chromium is oversimplified. It does not enter into the modeled
174 composition of pyroxenes and garnets (Asimow et al., 1995), which leads to an
175 overestimation of the range of conditions for which spinel can crystallize (e.g., Lambart et al.,
176 2009). In our calculations, we did include chromium due to the importance of spinel in the
177 reaction but we considered the overestimation of spinel in the interpretation of the results.
178 - pHMELTS offers a choice between two thermodynamic models for garnet. The older model
179 tends to overestimate the proportion of the grossular component (Berman & Koziol, 1991),
180 while the new one tends to overestimate the stability range for garnet (e.g, Elkins et al., 2019).
181 In our calculations, we used the older model of garnet but we performed calculations at a
182 maximum pressure of 2 GPa to avoid the garnet stability field.

- The solidus temperatures of peridotites are overestimated (Ghiorso et al., 2002).

2.2. The mixing model

We consider a simple model in which a subsolidus homogenous mantle domain composed of depleted peridotite (harzburgite) is impregnated by a finite amount of melt at constant pressure and temperature. The impregnation process is simulated by adding up to 50 g of melt by increments of 0.01 g, to 100 g of depleted peridotite. Each incremental addition of melt is followed by chemical re-equilibration of the impregnated peridotite. Lambart et al. (2012) used a similar approach to investigate the fate of pyroxenite-derived melt during interaction with the surrounding peridotite, with larger increments (5g). We do not model melt percolation, but simply melt-peridotite interaction during melt addition; the implications of this limitation are discussed below. Our model also does not aim to reproduce the physical aspects of the refertilization process. The actual amount of melt required during the refertilization process is controlled by factors such as the degree of disequilibrium (Oliviera et al., 2020), the mobility of the melt (Watson et al., 1990), the pressure gradient (Pec et al., 2015), or the grain size of the protolith (Turner et al., 2015). It is beyond the scope of this paper to test the effects of such parameters. Here we focus on the major element and modal composition of the solid phases after interaction.

2.2.1. Selected input parameters

Pressure, temperature and oxygen fugacity: We selected a range of oxygen fugacity (fO_2) between FMQ-3 and FMQ +3 (with FMQ standing for the fayalite-magnetite-quartz oxygen buffer) to look at the effects of oxygen fugacity variations around the average value for the oceanic lithosphere (Cottrell et al., 2021; Foley, 2011). Calculations were performed at 1.5 and 2 GPa, for temperatures (T) varying between 1150 and 1300°C, conditions corresponding to the subsolidus lithospheric mantle (Hirschmann, 2000). Under these conditions, silicate melts are expected to be strongly consumed during the reaction, for any realistic melt composition (Lambart et al., 2012). Details of the conditions for each test are given in **Table 1** (runs #1 to #12).

208 *Harzburgite compositions*: We selected three natural samples of depleted peridotites from the Lherz
209 massif (Roux et al. 2007) as starting compositions (**Table 2**). H1 corresponds to an average
210 harzburgite, H2 is slightly enriched in orthopyroxene, and H3 is orthopyroxene-rich.

211 *Melt compositions*: Several experimental studies have shown that a large part of the mineralogical and
212 compositional diversity in the mantle can be explained by melt-rock reactions (e.g., Kelemen et al.,
213 1990; Yaxley and Green, 1998; Morgan and Liang, 2003, 2005; Herzberg 2011; Lambart et al., 2012;
214 Mallik and Dasgupta, 2013; Soustelle et al., 2014; Mitchell & Grove, 2016). Le Roux et al. (2007)
215 suggested a refertilization process as a melt-rock reaction resulting in the dissolution of olivine and
216 crystallization of pyroxenes and spinel:

217 $$\text{Olivine} + \text{melt}_1 \rightarrow \text{Clinopyroxene} + \text{Orthopyroxene} + \text{Spinel} + \text{melt}_2 \qquad (1)$$

218 Not every melt, however, can trigger reaction (1) as the silica activity of the interacting melt must be
219 higher than the silica activity of the melt in equilibrium with the harzburgite protolith (Lambart et al.,
220 2012). If the silica activity is lower, clinopyroxene and olivine are produced at the expense of
221 orthopyroxene. For instance, Shaw et al. (2018) interpreted the formation of wehrlite as the result of
222 infiltration of orthopyroxene-undersaturated alkaline melt into the lithospheric mantle. The silica
223 activity calculated (Ghiorso et al., 1995) for the melt used in their model is low (e.g., $a_{liq}^{SiO_2} \sim 0.2$ at P
224 = 1.25 GPa and T =1350°C, and FMQ). In comparison, under similar conditions, the silica activity of
225 a melt in equilibrium with orthopyroxene and olivine is ~0.35 (Lambart et al., 2012).

226 In our calculations, we used three different basaltic melts (**Table 3**). The MOR melt is a basaltic
227 composition with a silica activity of 0.372, obtained in a partial melting experiment of a fertile
228 peridotite (Lambart et al., 2009) and corresponds to a spreading-ridge context. HS and HS2 are
229 picritic basalt compositions from Hawaii (Kilauea; Norman & Garcia, 1999) and Iceland (Reykjanes
230 Peninsula; Jakobsson, 1978), respectively. In our calculations, they represent primitive magmas from
231 hot spot contexts, with HS being more iron-rich than HS2. Unlike HS (which is olivine-rich), HS2
232 contains almost no phenocrysts and thus more closely represents a melt composition.

233 The silica activity of HS and HS2 melts are 0.485 and 0.551, respectively. Both of these melts have
234 higher silica activity than an experimental melt produced from partial melting of a fertile spinel
235 lherzolite at 2 GPa and 1375 °C, which has a value (i.e., 0.370; see KLB-1 run #21; Hirose &
236 Kushiro, 1993) very similar to that of the MOR melt.

237 For the P-T conditions chosen for the calculations, the liquid is completely, or very nearly (runs #3
238 and #5), consumed during the reaction. The strong consumption of silicate melt is partly due to the
239 overestimation of the solidus temperatures in pHMELTS (Ghiorso et al., 2002), regardless of the
240 composition (or silicate activity) of the melt and is also supported by experimental studies (e.g.,
241 Yaxley and Green, 1998; Lambart et al., 2012). It results in an enrichment of the incompatible
242 element concentration in the produced solid. When the liquid is absent after equilibration, the system
243 can be viewed as a two-component mixture between the depleted peridotite and the added melt.

244 As the melt consumption is usually accompanied by the precipitation of clinopyroxene
245 (+orthopyroxene/olivine), it results in a local decrease in the permeability of the system. Lambart et
246 al. (2012) suggested that such permeability decrease might result in the affected lithology evolving as
247 a near-closed system, similar to what is modeled here. Nevertheless, a silicate melt in mineralogical
248 assemblages dominated by olivine can however become interconnected at a very low melt fraction
249 (e.g., Waff & Faul, 1992; Zhu et al., 2011; Laumonier et al., 2017), and a real closed system is
250 unlikely. The escape of a small melt fraction has however very little impact on the behavior of
251 elements with an affinity for the solid phase (i.e., the compatible elements), but can significantly
252 affect elements preferentially partitioning into the melt phase (i.e., incompatible elements). The latter
253 should thus be preferred if we are to characterize the open/closed character of the process. In order to
254 test the impact of the presence of a melt phase on the incompatible element concentrations of the
255 coexisting solid phase, we also performed a run with a liquid phase present (run #12, **Table 1**).
256 Calculations were performed at T = 1400°C, an unlikely temperature for the continental lithosphere,
257 which forced the resulting system to have a melt phase. In this melt-present run, the incompatible
258 elements are partitioned into the melt phase during each step of the modeled process. While the closed
259 system approximation underscores the simplicity of our model and its limited applicability to

incompatible element concentrations, in many aspects our calculations may be representative of a process of simple impregnation of a refractory peridotite by a silicate melt in the continental mantle lithosphere.

2.3. The partial melting model

In order to compare with the impregnation model, we also performed 3 partial melting simulations (runs PM1, PM2 and PM3, **Table 1**). We used the Primitive Upper Mantle composition from McDonough (1995) as a starting composition (PUM in **Table 2**). Run PM1 was performed at constant pressure (2 GPa), with a temperature rising from 1200 to 1520°C. Run PM2 was performed at constant temperature (1230°C), with pressure decreasing from 2 to 0.6 GPa. Finally, run PM3 was performed at constant entropy, with pressure decreasing from 2 to 0.6 GPa, and starting temperature of 1396°C (PUM solidus temperature at 2 GPa), in order to model more geodynamically realistic conditions. As the melt remains in contact with the residue throughout the simulations, all three of these cases can be viewed as thermodynamically constrained batch melting models.

3. Results

We focus on the solid bulk composition and modal proportions of the solid phase and do not consider mineral phase compositions. In fact, inter-mineral partitioning of major element components such as Fe-Mg in the lithospheric mantle is strongly dependent on the equilibration temperature (Brey and Köhler, 1990). As thermal reequilibration is the rule in lithospheric domains, comparing the elemental compositions of the individual phases obtained from our thermodynamic model outputs with natural data would not produce meaningful results. Bulk residual assemblage compositions and modal proportions are less significantly affected by the temperature of reequilibration, and we present the corresponding results hereafter.

3.1. Reference simulation (run #1)

The main results of the mixing models are the evolutions of modal proportions (**Figs. 2, 3, Table 4, and Supplementary Fig. S1**), and of bulk solid assemblage compositions (**Fig. 4 and 5**). We will use

the outputs of run#1 as a reference for comparison with other tests. Results for this run show production of spinel (+2.5), orthopyroxene (+0.2), and clinopyroxene (+28.6), with the values indicating the absolute change in the modal proportion of each phase (normalized to 100). In contrast, the liquid is totally consumed and olivine proportion also diminishes (-31.3) (**Fig. 2**). This decrease in olivine proportion is not due solely to the precipitation of the other phases but also to olivine dissolution (Fig. 2b). Initial harzburgite is hence progressively modified to clinopyroxene-rich harzburgite, and eventually to a lherzolite assemblage (**Fig. 3**). As no liquid is present after equilibration, the bulk chemical composition of the solid assemblage (**Fig. 4**) evolves along mixing lines between the composition of the initial peridotite and the composition of the melt. Therefore, for run#1, after addition of 50% liquid, the bulk chemical composition shows an enrichment in Al_2O_3 (+5.4 wt.%), CaO (+3.8 wt.%), SiO_2 (+1.6 wt.%), and Na_2O (+1 wt.%), a decrease in MgO (-11.7 wt.%), and a slight decrease in FeO_t (-0.3 wt.%) (FeO_t: total iron content expressed as FeO).

3.2. Influence of the impregnation conditions

The effect of variations of P, T, and redox parameters on the model results are presented in **Fig. 3a**. Runs #1, #3 and #4 illustrate the effect of temperature on the reaction (T = 1230, 1300, and 1150°C, respectively), runs #1 and #5 are used to investigate the effect of a small variation of pressure (P = 2 and 1.5 GPa, respectively). Runs #1, #6a, #6b, #7a and #7b are used to track the effect of redox conditions on the reaction (fO_2 = FMQ, FMQ+1, FMQ+3, FMQ-1, and FMQ-3, respectively). In all of these cases, the same initial peridotite composition and the same melt composition were used (H1; MOR). The effect of pressure and temperature is insignificant for the ranges considered in this study (**Fig. 3a**). Additionally, for most of the fO_2 conditions tested here, the modal proportions of the impregnated peridotite strongly overlap with each other. Under highly oxidized conditions (i.e., run #6b: FQM+3) however, 4.9 wt.% of orthopyroxene is produced at the expense of olivine (-35.3 wt.%). This is because Fe^{3+} is not easily incorporated in olivine and a higher Fe^{3+}/Fe^{2+} ratio will favor the dissolution of olivine and precipitation of pyroxene.

3.3. Influence of the composition

311 The influence of the melt composition on the refertilization process was tested in runs #1, #2 and #11
312 (MOR, HS, and HS2, respectively). The influence of the initial peridotite composition was tested in
313 runs #1, #8 and #9 (H1, H2, and H3, respectively). Run #10 also investigates a variation of both
314 starting material composition (H3) and melt composition (HS). These six runs are displayed in **Figs.**
315 **3b, 3c and 4**. Because the melt is consumed during the reaction, bulk compositions follow mixing
316 lines between the composition of the initial peridotite and the composition of the melt (**Fig. 4**). In the
317 major element diagrams (**Fig. 4**), this results in solid assemblages with greater sodium and calcium
318 enrichments for models performed with MOR addition, and slightly greater iron enrichment for
319 models performed with HS addition, relative to that performed with HS2 addition, directly reflecting
320 the differences in melt compositions (**Table 3**). In the Streckeisen projections (**Fig 3b**), the addition of
321 the HS2 melt (run #11) results in a strong orthopyroxene enrichment and the final lithology (after
322 50% melt addition) is an orthopyroxene-rich olivine websterite (35% olivine. 52% orthopyroxene, 9%
323 clinopyroxene). On the contrary, the reaction with the MOR melt (run #1) results in both
324 clinopyroxene and orthopyroxene enrichments, but the final lithology is in the field of lherzolite (49%
325 olivine. 20% orthopyroxene, 29% clinopyroxene). The addition of HS melt (run #2) results in a near-
326 vertical trend in the Streckeisen diagram with a final lithology in the field of lherzolite with a similar
327 proportion of olivine but a higher orthopyroxene/clinopyroxene ratio (49% olivine. 30%
328 orthopyroxene, 20% clinopyroxene). Finally, the main effect of varying the initial harzburgite
329 composition is to change the initial location of the mixing trend, that is the orthopyroxene/olivine
330 ratio in the Streckeisen projection (**Fig. 3c**). Runs #1 and #8 evolve from the domain of harzburgites
331 to lherzolites, and run #9 to websterites.

332 **3.4. Other runs**

333 **3.4.1 Partial melting runs**

334 Partial melting simulations PM1, PM2 and PM3 are presented in **Fig. 3d** and **Fig. 5**. The end of run
335 PM1 corresponds to an amount of liquid produced of 30 wt.% (**Table 4, Supplementary Fig. S1n**),
336 while the ends of PM2 and PM3 correspond to 7 wt.% and 5 wt.% of liquid produced, respectively

(**Supplementary Figs. S1o and S1p**). The low amount of melt produced in PM2 and PM3 is due to the overestimation of the solidus temperature of the peridotite in pHMELTS (Ghiorso et al., 2002). In the partial melting run at constant pressure (PM1), as the temperature rises above the PUM (Primitive Upper Mantle; McDonough, 1995) solidus temperature at 2 GPa (1296°C), clinopyroxene is strongly consumed (-22 modal %) corresponding to a change in lithology from lherzolite to harzburgite (**Fig. 3d)**. The chemical composition of the residual solid shows a final enrichment in MgO (+6 wt.%), and SiO_2 (+0.8 wt.%), associated with a decrease in Al_2O_3 (-2.5 wt.%), CaO (-2.5 wt.%), FeO_t (-1.4 wt.%), and Na_2O (-0.3 wt.%), with values representing absolute changes in the proportions of these species in the solid phase. In the plot of Na_2O vs. Al_2O_3 a curved trend is observed, which starts out steeply at Al_2O_3 contents > 4 wt.%, and Na_2O contents > 0.1 wt.% and flattens out with continued melting (**Fig. 5**).

The partial melting run under conditions of isentropic decompression (PM3) also starts at 1296°C. pHMELTS adapts the temperature during the simulation in order to maintain constant entropy (down to 1214°C). By the end of the run, olivine has been produced (+2.4%) at the expense of clinopyroxene (-8.6 %) (**Fig. S1p**). However, in detail some complexity is observed as pressure decreases. At first the formation of orthopyroxene (+1.6 %) is slightly favored over that of olivine (+1.1%), but starting at around 0.8 GPa, the orthopyroxene/olivine ratio shows a progressive decrease, as olivine production is favored in comparison to orthopyroxene (**Fig. 3d**), consistent with the increasing stability of olivine with decreasing pressure (Stolper, 1980). The chemical composition of the residual solid shows an enrichment in MgO (+2 wt.%) and FeO_t (+0.2 wt.%), and a decrease in Al_2O_3 (-1 wt.%), SiO_2 (-0.6 wt.%), CaO (-0.3 wt.%), and Na_2O (-0.3 wt.%) (**Fig. 5**).

The partial melting run by decompression at constant T (PM2) shows similar evolution to that at constant entropy (PM3). Olivine is produced (+3%) at the expense of clinopyroxene (-5.5%) and orthopyroxene (-4.3%) (**Fig. 3d** and **Supplementary Fig. S1o**). The residual solid is enriched in MgO (+2.36 wt.%) and FeO_t (+0.25 wt.%), and depleted in Al_2O_3 (-1.2 wt.%), SiO_2 (-0.7 wt.%), CaO (-0.4 wt.%), and Na_2O (-0.28 wt.%) (**Fig. 5**). In runs PM2 and PM3, the relatively limited change in bulk

363 composition, which does not attain the harzburgite field, is likely due to the overestimation of the
364 solidus temperature in pHMELTS noted above.

365 **3.4.2. Liquid-present run**

366 In most respects, the liquid-present run#12 (**Figs. 3d and 5**) shows a similar trend to the runs
367 performed at lower temperature. A notable exception is Na content, which is less enriched in the
368 refertilized assemblage than in the melt-free models (+0.4 wt.% for run #12, compared to +1 wt.% for
369 the reference run). This is because Na is strongly partitioned into the liquid phase. The final
370 percentage of melt in the assemblage is 7.5 wt.%. Minor amounts of liquid are also present in runs #3
371 (1300°C) and #5 (1.5GPa) and these also show a slightly lower Na enrichment in the solid assemblage
372 than in the melt-free runs. Nevertheless, the final melt fractions being 0.9 wt.% and 1.6 wt.%
373 (respectively) in these runs, the variation of the Na content compared to the reference simulation is
374 not significant (+0.8 wt.% and +0.7 wt.% for runs #3 and #5 respectively, compared to +1 wt.% for
375 the reference run). For the other chemical elements, these two runs show similar trends to those of the
376 reference run.

377 **4. Discussion**

378 Refertilization of the SCLM is a complex phenomenon that likely involves numerous agents and
379 mechanisms. Nevertheless, our model confirms that the reaction: Olivine + $melt_1$ → Clinopyroxene +
380 Orthopyroxene + Spinel + $melt_2$ suggested based on petrological grounds (e.g., Le Roux et al., 2007)
381 is thermodynamically possible, and thus supports its key participation in the refertilization process.
382 The composition of the infiltrating melt has a first-order control on the range of chemical and
383 mineralogical compositions observed in the SCLM.

384 **4.1. Natural data**

385 Most ophiolitic and abyssal peridotites are represented by harzburgitic lithologies (e.g., Bodinier and
386 Godard, 2014). On the contrary, peridotites from the sub-continental lithosphere, particularly orogenic
387 peridotites and ultramafic xenoliths from non-cratonic terrains, encompass many lherzolitic

lithologies (**Fig. 3**). There is substantial scatter in natural peridotite chemical compositions (**Fig. 4 and 5**). However, most natural compositions define a broad trend, with increasing SiO_2, CaO, Al_2O_3 and Na_2O contents, coupled with decreasing MgO content and relatively constant FeO content. Some of the scatter in modal and chemical composition in lithospheric peridotites could be due to inherited heterogeneity from the convecting mantle, related to crustal recycling, convection and melting, and melt-solid interactions beneath the ridges and at hot spots (e.g., Sobolev et al., 2005), or various degrees of partial melting under various conditions (e.g., melting at different pressures; Olivera et al., 2020; Tomlinson & Kamber, 2021). Also temperature reequilibration could trigger noticeable modal variations is some specific samples (e.g., two-pyroxene exsolutions, pyroxene exsolution from garnet, spinel exsolution from clinopyroxene; Kornprobst et al., 1990; France et al., 2015), which could also trigger scatter in the database, and that would eventually hamper direct comparison with our model outputs for those specific samples. However, the presence of a trend in major element compositions (**Figs. 4 and 5**) strongly suggests a genetic link between refractory (i.e., harzburgite) and fertile (i.e., lherzolite) lithologies. The goal of the following exercise is not to reproduce the full spectrum of natural compositions but to test whether our thermodynamic mixing model is consistent with this potential genetic link, and discuss which parameters in our model are the most likely to explain the spectrum of compositions observed in natural peridotites.

In **Figures 3, 4 and 5**, we compare the results of our thermodynamic mixing models with the global database for tectonically emplaced peridotites, including orogenic, ophiolitic and abyssal peridotites (Bodinier and Godard, 2014). Our results show that most of the wide range of modal proportions in lherzolite can be reproduced by our model of impregnation of harzburgitic lithologies by silicate melts. In addition, it is clear from **Fig. 3** that further impregnation would make the impregnated peridotite enter the domain of websterites, rocks composed essentially of orthopyroxene and clinopyroxene, and less than 40% olivine. This suggests that very extensive refertilization could be at the origin of some websterite and pyroxenites, and that harzburgites, lherzolites and pyroxenites may form a continuum rather than distinct groups. Such a continuum is commonly reported in mantle series and mainly explained by melt-rock reactions (e.g., from clinopyroxenite to orthopyroxenite in

Kornprobst, 1969; from dunite to lherzolite in Morgan and Liang, 2005; from dunite to websterite in Denis et al., 2018, or from harzburgite to websterite in Lambart et al., 2022). The simple impregnation model presented here however, is unlikely to explain the scatter in the most refractory lithologies (i.e., olivine-rich harzburgite and dunite). Indeed, scatter in natural peridotite compositions (**Figs. 4 and 5**) exceeds the range of variation in our impregnation model with some rare peridotites showing very high CaO/Al_2O_3 ratio or high FeO (>10 wt.%) concentrations. However, most of the natural compositions and the impregnation model results follow similar chemical trends. The effects of each input parameter of the model are discussed below.

4.2. Influence of varying parameters on the refertilization products

The impregnation models presented here highlight that variations of temperature and redox conditions, as well as small pressure variations have almost no impact on the evolution of the system in terms of modal composition (**Fig. 3a**). Hereafter we first discuss the two main parameters that influence the evolution of the system in our calculations: the composition of the percolating melt, and to a lesser extent the composition of the percolated harzburgite.

4.2.1. Percolated harzburgite composition

Although significant scatter is present in the natural data when compared to our models, our results show that a refertilization process has the potential to reproduce the harzburgite - lherzolite suites. The scatter in the orthopyroxene/olivine ratio in natural lherzolite series could be explained by a variation of the orthopyroxene/olivine ratio in the initial harzburgite (**Fig. 3c**). This scenario would require a large preexisting compositional variability of the refractory mantle, *before* impregnation. Harzburgite H3, for instance, is an orthopyroxene-rich harzburgite with a very low calcium content compared to aluminum that can be viewed as an extreme orthopyroxene-rich end-member.

Several processes could explain the origin of such compositional variability (variations of the orthopyroxene/olivine ratio). For instance, in the decompression runs (PM2 and PM3), the stabilities of olivine and orthopyroxene during the melting reaction change with pressure. The coexistence of

various residual harzburgites formed by partial melting at different pressures could result in different orthopyroxene/olivine ratios. The preexisting heterogeneity could also be due to the delamination of the cratonic lithospheric mantle into the convecting mantle, be a natural consequence of oceanic crust subduction into the convecting mantle, or result from the interaction of peridotite with an eclogite or pyroxenite-derived melt (e.g., Yaxley and Green, 1998; Tomlinson & Kamber, 2021).

4.2.2. Percolating melt composition

For the following discussion, we used H1, a typical harzburgite (**Table 2**) as the starting composition to examine the effect of melt composition on the output of the impregnation modeling (**Figs. 3b and 4**). Because all three percolating melts have high silica activities (**Table 3**), in all cases the proportion of pyroxenes increases during melt impregnation. However, the clinopyroxene/orthopyroxene ratio is strongly affected by the Ca content of the melt with more clinopyroxene produced for Ca-rich melts (**Table 3**, **Fig. 3b**). In addition to being Ca-poor, HS2 is also more Si-rich than the two other basalt compositions, resulting in more efficient crystallization of pyroxene, particularly orthopyroxene, at the expense of olivine (**Fig. 3b and Supplementary Fig. S1l**). This results in a final mineralogical assemblage for run #11 in the field of orthopyroxene-rich olivine websterite.

Except for the liquid-present run (run #12), the melt phase is entirely, or almost entirely (runs #3 and #5; **Supplementary Fig. S1b and S1d**), consumed during the impregnation process (**Table 4**). This implies that the bulk composition of the percolated peridotite evolves along a mixing trend between the starting harzburgite and the melt composition (**Fig. 4**). We note that melt HS2 is too Ca-poor to reproduce the trend of natural compositions. Additionally, part of the vertical scatter for all oxides in **Fig. 4** cannot be explained by our impregnation model (especially for ophiolitic and abyssal peridotites; e.g., variation of SiO_2 content for a given Al_2O_3 content). Finally, for the three melt compositions tested here, the modeled Na_2O vs. Al_2O_3 enrichment trend is much steeper than the correlation observed in the natural dataset (**Fig. 4**). As described in sections 2.2.1 and 3.4.2, this is due to the full consumption of liquid during the reaction, which likely differs from olivine-dominated systems in which a small fraction of liquid is expected to leave the system during melt percolation

(see reaction *(1)*). Without this liquid phase, elements that partition preferentially into the melt phase such as Na remain in the solid phases (**Fig. 4**). On the contrary, in the presence of a liquid phase (run #12), Na preferentially partitions into the melt resulting in a much lower increase of the Na_2O content in the solid phase during the impregnation process (**Fig. 5**), similar to the trend observed in natural data. In the liquid-present run, the final melt fraction in the system at equilibrium is about 7.5 wt.%. In natural systems, which may be seen as chromatographic percolation columns (e.g., Navon and Stolper, 1987), significantly lower instantaneous melt fractions can explain the low contents of Na in the solid phase. Chemical disequilibrium during melt transport also favors stronger partitioning of Na into the melt phase (Oliveira et al., 2020). In any case our results support the supposition that refertilization is an open system process.

4.3. Comparison with partial melting

Partial melting processes can also produce refractory lithologies (**Fig. 3d** and **Fig. 5**). However, our partial melting models do not fully reproduce the spectrum of compositions observed in non-cratonic continental peridotites (**Fig. 3d** and **Fig. 5**). In addition, our mixing model tended to reproduce the rough linear trend represented by the spectrum of natural continental lithospheric data more faithfully than our simplified partial melting model (straight line vs. curved lines for runs PM2 and PM3 in **Fig 3d**). Previous authors (e.g. Niu, 1997) have also pointed out that mixing more successfully reproduces linear trends (FeO vs. MgO and SiO_2 vs MgO) in peridotites than partial melting alone. We note however, that more complex dynamic melting models, such as that of Oliveira et al. (2020) which takes into consideration disequilibrium behavior, heterogeneous source compositions and melt transport rates, can produce a wider variety of compositions than the partial melting runs performed in this study (**Fig. 3d**).

As highlighted in **Fig.1**, partial melting and refertilization likely both contribute to producing lithospheric heterogeneities. Furthermore, refertilization and partial melting sometimes may be genetically linked, as the near absence of lherzolites with unradiogenic osmium isotope compositions in the non-cratonic lithosphere argues that refertilization usually occurs soon after harzburgite

492 formation (Rudnick & Walker, 2008; Reisberg, 2021). This implies that the original partial melting
493 episodes may potentially be causally linked to subsequent refertilization, which could result from
494 percolation of the remaining melts through the cooling lithosphere. We stress that refertilization as
495 used here refers to the process of transformation of harzburgite by interaction with silicate melt in the
496 non-cratonic mantle lithosphere. This can produce clinopyroxene-enriched harzburgite, lherzolite, or
497 other types of peridotite depending on the percolating melt composition. Other refertilization
498 processes, often referred to broadly as metasomatic (e.g., circulation of various silicate melts, or of
499 hydrous, carbonatitic, or kimberlite fluids/melts) also very frequently affect both the cratonic (e.g.,
500 Song and Frey, 1989; Griffin et al., 1999; Jollands et al., 2018) and the non-cratonic lithosphere (e.g.,
501 Menzies and Dupuy, 1991; Baker et al., 1998; Raffone et al., 2009; Gu et al., 2018; Azevedo-Vannson
502 et al., 2021). Such processes can lead to enrichment of major or incompatible element abundances,
503 water contents, modification of isotope compositions and/or localized phase precipitation, and can
504 occur at various times throughout the history of a lithospheric domain.

505 **4.4. Other parameters.**

506 One of the goals of our study was to determine the first-order parameters controlling the
507 compositional and modal variability of the SCLM. Unsurprisingly, the melt and the protolith
508 compositions have the strongest effect on the evolution of the system. However, because of the
509 simplicity of our model, the effects of other parameters (e.g., fO_2, presence of volatiles, chemical
510 disequilibrium), may be underestimated. Here we briefly review the potential effects of additional
511 parameters.

512 Our results show that highly oxidized melts result in slightly higher olivine dissolution and slightly
513 higher pyroxene (mostly orthopyroxene) precipitation compared to the reference run (see run #6b:
514 **Fig. 3a**). Such high degrees of oxidation have been encountered in some oceanic island xenoliths
515 (Cottrell et al., 2021) and might reflect the interaction of the xenolith with a hydrous melt (e.g.,
516 Bryant et al., 2007). However, for most conditions relevant to the lithospheric mantle, and in the
517 major melting regime considered in this study, the effect of fO_2 seems to be insignificant. These

518 results are consistent with Shaw et al. (2018). In their calculations, an increase in the fO_2 from FQM-2
519 to FQM+2 resulted in a small decrease of the olivine/orthopyroxene ratio in the initial lithology but
520 the effect of variable fO_2 on the output of the reaction was negligible.

521 The addition of volatiles (H_2O or CO_2) is expected to significantly decrease the solidus temperature of
522 the system (e.g., Asimow and Langmuir, 2003; Dasgupta and Hirschmann, 2006). Hence, based on
523 temperature considerations only, we could expect that a refertilizing hydrous or carbonated melt
524 would result in lower consumption of melt during the reaction. However, this is not supported by
525 experiments. Mallik and Dasgupta (2013) performed reaction experiments between a lherzolite and a
526 CO_2-bearing basaltic andesite melt. In comparison to similar CO_2-free experiments, the addition of
527 CO_2 to the reacting melt has little to no effect on the proportion of residual melt after the reaction.
528 This likely is because the addition of volatiles in the melt increases the reactivity and disequilibrium
529 degree of the melt, resulting in a highly dynamic dissolution-precipitation process (e.g., Keller and
530 Katz, 2016; Lambart et al., 2022; Mallmann et al., 2009; Shaw et al., 2018). Additionally, in
531 comparison to CO_2-free experiments, Mallik and Dasgupta (2013) observed an increase in
532 orthopyroxene (and garnet) in the residual solid after reaction at the expense of olivine and
533 clinopyroxene. Similarly, Wang et al. (2016) demonstrated that the reaction of a hydrous melt with a
534 lherzolite can produce orthopyroxenite. Hence, although orthopyroxene stability also strongly
535 depends on the silica activity of the melt, the addition of volatiles may result in shifting the
536 compositional effect of the melt towards orthopyroxene-rich lithologies (**Fig. 3**). However, the effect
537 of volatiles is likely limited in comparison to that of the major-element composition of the melt. In
538 fact, in the Mallik and Dasgupta (2013) study, similar experiments performed with an alkali basalt
539 melt, but with a CO_2 content more than four times higher than that of the basaltic andesite melt result
540 in much lower consumption of olivine for a similar consumption of melt.

541 Oliveira et al. (2020) demonstrated that the degree of chemical disequilibrium during partial melting
542 can significantly modify the compositional trends of major elements observed in basalt when
543 compared with equilibrium calculations. As these authors noted, disequilibrium polybaric melting
544 increases the fractionation of Na into the melt phase. In their calculations however, both equilibrium

and disequilibrium models produced similar modal evolution of the residual mantle (**Fig. 3d**). The effect of variable potential temperature of the mantle can result in slightly larger variability, but mostly because it results in changing the initial mineralogical composition of the lherzolite between the spinel and the garnet stability field.

5. Conclusions

In order to test the hypothesis of lherzolite formation by refertilization of the non-cratonic continental mantle lithosphere, we employed a simple thermodynamic mixing model of harzburgite with a silicate melt of tholeiitic to picritic composition. We independently investigated the influence of various thermodynamic parameters (pressure, temperature, redox conditions, and the chemical composition of initial peridotite and percolating melt) on the chemical and modal compositions of the resulting lithology. Despite their simplicity, our calculations show that a large part of the compositional variability observed in orogenic peridotites can be explained by the impregnation of a refractory harzburgitic lithospheric mantle with silicate melt of various compositions. We also show that temperature, oxygen fugacity, and small variations of pressure have almost no impact on the evolution of the modal composition of the system; melt composition and initial harzburgite composition are the most influential thermodynamic parameters. The latter directly control the refertilization reaction and so, the phase proportions. To reproduce the natural compositional variability of continental peridotites, initial compositional heterogeneity of the harzburgitic protoliths is needed, as well as impregnation with various silicate melts. The three liquid compositions used here represent a range of mantle melts that could serve as potential refertilizing agents. Our run #2 with an initial average harzburgitic composition (H1) and a picritic basaltic melt (HS) best reproduced the broad trend of the natural data, but other protolith-melt combinations could also explain some of the natural variability. For instance, the composition of a liquid depends on its geodynamic context, which controls the pressure and temperature of melting, as well as the composition of the source. Finally, we highlighted that the main limitation of our model is that the refertilization process is treated as simple melt impregnation rather than melt percolation. The elements that partition preferentially into the melt phase (represented here by Na) are removed from the rock during melt percolation in the natural

system. Our thermodynamic mixing model cannot reproduce this strong fractionation of incompatible elements in the liquid phase during reactive infiltration as in our model, the melt phase is completely consumed in the reaction. This leads to an enrichment of incompatible elements in the resulting lithology in the model, and underscores the open system character of the natural refertilization process. Despite this drawback, our calculations provide thermodynamic support for models suggesting that much of the variability in the major element and modal compositions of the natural data can be reproduced by the impregnation of a harzburgite with silicate melts of various compositions.

Acknowledgments

We thank the reviewers, Cliff Shaw and Romain Tilhac, for their constructive comments, as well as Sonja Aulbach for her editorial handling, which greatly improved the quality of this manuscript. LF thanks Pierre Bouilhol, Jean-Louis Bodinier, and Valentin Casola for constructive discussions related to mantle refertilization. This work was supported by the French National Research Agency through the project GECO-REE (ANR-16-CE01-0003-01; P.I., LF). SL acknowledges funding support from NSF grant EAR-1946346. This is CRPG contribution number xxxx, and GECO-REE contribution number yy.

References

Allègre, C. J., & Turcotte, D. L. (1986). Implications of a two-component marble-cake mantle. Nature, 323(6084), 123-127. https://doi.org/10.1038/323123a0

Armytage, R. M. G., Brandon, A. D., Peslier, A. H., & Lapen, T. J. (2014). Osmium isotope evidence for Early to Middle Proterozoic mantle lithosphere stabilization and concomitant production of juvenile crust in Dish Hill, CA peridotite xenoliths. Geochimica et Cosmochimica Acta, 137, 113-133. https://doi.org/10.1016/j.gca.2014.04.017

Asimow, P. D., Dixon, J. E., & Langmuir, C. H. (2004). A hydrous melting and fractionation model for mid-ocean ridge basalts□: Application to the Mid-Atlantic Ridge near the Azores: HYDROUS MELTING AND FRACTIONATION. Geochemistry, Geophysics, Geosystems, 5(1), n/a-n/a. https://doi.org/10.1029/2003GC000568

Asimow, P. D., & Ghiorso, M. S. (1998). Algorithmic modifications extending MELTS to calculate subsolidus phase relations. American Mineralogist, 83(9-10), 1127-1132. https://doi.org/10.2138/am-1998-9-1022

Asimow, P. D., & Langmuir, A. C. (2003). The importance of water to oceanic mantle melting regimes. Nature, 421(6925), 815-820.

Asimow, P. D., Hirschmann, M. M., Ghiorso, M. S., O'Hara, M. J., & Stolper, E. M. (1995). The effect of pressure-induced solid-solid phase transitions on decompression melting of the mantle. Geochimica et Cosmochimica Acta, 59(21), 4489-4506. https://doi.org/10.1016/0016-7037(95)00252-U

Azevedo-Vannson, S., France, L., Ingrin, J., Chazot, G. (2021) Mantle metasomatic influence on water contents in continental lithosphere: New constraints from garnet pyroxenite xenoliths (France & Cameroon volcanic provinces). Chemical Geology, 575, 1202257.

Baker, J., Chazot, G., Menzies, M., & Thirlwall, M. (1998). Metasomatism of the shallow mantle beneath Yemen by the Afar plume—Implications for mantle plumes, flood volcanism, and intraplate volcanism. *Geology*, *26*(5), 431. https://doi.org/10.1130/0091-7613(1998)026<0431:MOTSMB>2.3.CO;2

Berman, R. G., & Koziol, A. M. (1991). Ternary excess properties of grossular-pyrope-almandine garnet and their influence in geothermobarometry. American Mineralogist, 76(7-8), 1223-1231.

Beyer, E. E. (2006). Transformation of Archaean Lithospheric Mantle by Refertilization□: Evidence from Exposed Peridotites in the Western Gneiss Region, Norway. Journal of Petrology, 47(8), 1611-1636. https://doi.org/10.1093/petrology/egl022

Bodinier, J.-L., Garrido, C. J., Chanefo, I., Bruguier, O., & Gervilla, F. (2008). Origin of Pyroxenite-Peridotite Veined Mantle by Refertilization Reactions□: Evidence from the Ronda Peridotite (Southern Spain). Journal of Petrology, 49(5), 999-1025. https://doi.org/10.1093/petrology/egn014

Bodinier, J.-L., & Godard, M. (2003). Orogenic, Ophiolitic, and Abyssal Peridotites. In Treatise on Geochemistry (p. 1-73). Elsevier. https://doi.org/10.1016/B0-08-043751-6/02004-1

Bodinier, J.-L., & Godard, M. (2014). Orogenic, Ophiolitic, and Abyssal Peridotites. In Treatise on Geochemistry (p. 103-167). Elsevier. https://doi.org/10.1016/B978-0-08-095975-7.00204-7

Borghini, G., Rampone, E., Class, C., Goldstein, S., Cai, Y., Cipriani, A., Hofmann, A. W., & Bolge, L. (2021). Enriched Hf Nd isotopic signature of veined pyroxenite-infiltrated peridotite as a possible source for E-MORB. Chemical Geology, 586, 120591. https://doi.org/10.1016/j.chemgeo.2021.120591

Borghini, G., Rampone, E., Zanetti, A., Class, C., Fumagalli, P., & Godard, M. (2020). Ligurian pyroxenite-peridotite sequences (Italy) and the role of melt-rock reaction in creating enriched-MORB mantle sources. Chemical Geology, 532, 119252. https://doi.org/10.1016/j.chemgeo.2019.07.027

Brey, G. P., & K Hler, T. (1990). Geothermobarometry in Four-phase Lherzolites II. New Thermobarometers, and Practical Assessment of Existing Thermobarometers. Journal of Petrology, 31(6), 1353-1378. https://doi.org/10.1093/petrology/31.6.1353

Byerly, B. L., & Lassiter, J. C. (2012). Evidence from mantle xenoliths for lithosphere removal beneath the central Rio Grande Rift. Earth and Planetary Science Letters, 355-356, 82-93. https://doi.org/10.1016/j.epsl.2012.08.034

Bryant, J. A., Yogodzinski, G. M., & Churikova, T. G. (2007). Melt□mantle interactions beneath the Kamchatka arc: Evidence from ultramafic xenoliths from Shiveluch volcano. Geochemistry, Geophysics, Geosystems, 8(4).

Chazot, G., Menzies, M., & Harte, B. (1996). Silicate glasses in spinel lherzolites from Yemen□: Origin and chemical composition. Chemical Geology, 134(1-3), 159-179. https://doi.org/10.1016/S0009-2541(96)00086-1

Cottrell, E., Birner, S. K., Brounce, M., Davis, F. A., Waters, L. E., & Kelley, K. A. (2021). Oxygen Fugacity Across Tectonic Settings. In R. Moretti & D. R. Neuville (Éds.), Geophysical Monograph Series (1□□ éd., p. 33-61). Wiley. https://doi.org/10.1002/9781119473206.ch3

Dai, H.-K., Zheng, J.-P., Griffin, W. L., O'Reilly, S. Y., Xiong, Q., Ping, X.-Q., Chen, F.-K., & Lu, J.-G. (2021). Pyroxenite Xenoliths Record Complex Melt Impregnation in the Deep Lithosphere of the Northwestern North China Craton. Journal of Petrology, 62(2), egaa079. https://doi.org/10.1093/petrology/egaa079

Dasgupta, R., & Hirschmann, M. M. (2006). Melting in the Earth's deep upper mantle caused by carbon dioxide. Nature, 440(7084), 659-662.

Denis, C. M. M., Demouchy, S., & Alard, O. (2018). Heterogeneous hydrogen distribution in orthopyroxene from veined mantle peridotite (San Carlos, Arizona)□: Impact of melt-rock interactions. *Lithos*, *302-303*, 298-311. https://doi.org/10.1016/j.lithos.2018.01.007

Dick, H. J. B., Fisher, R. L., & Bryan, W. B. (1984). Mineralogic variability of the uppermost mantle along mid-ocean ridges. Earth and Planetary Science Letters, 69(1), 88-106. https://doi.org/10.1016/0012-821X(84)90076-1

Downes, H., Bodinier, J.-L., Thirlwall, M. F., Lorand, J.-P., & Fabries, J. (1991). REE and Sr-Nd Isotopic Geochemistry of Eastern Pyrenean Peridotite Massifs□: Sub-Continental Lithospheric Mantle Modified by Continental Magmatism. Journal of Petrology, Special_Volume(2), 97-115. https://doi.org/10.1093/petrology/Special_Volume.2.97

Elkins, L. J., Bourdon, B., & Lambart, S. (2019). Testing pyroxenite versus peridotite sources for marine basalts using U-series isotopes. Lithos, 332-333, 226-244. https://doi.org/10.1016/j.lithos.2019.02.011

Elthon, D. (1992). Chemical trends in abyssal peridotites□: Refertilization of depleted suboceanic mantle. Journal of Geophysical Research, 97(B6), 9015. https://doi.org/10.1029/92JB00723

Foley, S. F. (2011). A Reappraisal of Redox Melting in the Earth's Mantle as a Function of Tectonic Setting and Time. Journal of Petrology, 52(7-8), 1363-1391. https://doi.org/10.1093/petrology/egq061

France, L., Chazot, G., Kornprobst, J., Dallai, L., Vannucci, R., Grégoire, M., Bertrand, H., & Boivin, P. (2015). Mantle refertilization and magmatism in old orogenic regions□: The role of late-orogenic pyroxenites. Lithos, 232, 49-75. https://doi.org/10.1016/j.lithos.2015.05.017

Frey, F. A., John Suen, C., & Stockman, H. W. (1985). The Ronda high temperature peridotite□: Geochemistry and petrogenesis. Geochimica et Cosmochimica Acta, 49(11), 2469-2491. https://doi.org/10.1016/0016-7037(85)90247-9

Frey, F. A., & Prinz, M. (1978). Ultramafic inclusions from San Carlos, Arizona□: Petrologic and geochemical data bearing on their petrogenesis. Earth and Planetary Science Letters, 38(1), 129-176. https://doi.org/10.1016/0012-821X(78)90130-9

Gao, S., Rudnick, R. L., Carlson, R. W., McDonough, W. F., & Liu, Y.-S. (2002). Re–Os evidence for replacement of ancient mantle lithosphere beneath the North China craton. Earth and Planetary Science Letters, 198(3-4), 307-322. https://doi.org/10.1016/S0012-821X(02)00489-2

Garrido, C. J., & Bodinier, J.-L. (1999). Diversity of Mafic Rocks in the Ronda Peridotite□: Evidence for Pervasive Melt-Rock Reaction during Heating of Subcontinental Lithosphere by Upwelling Asthenosphere. Journal of Petrology, 40(5), 729-754. https://doi.org/10.1093/petroj/40.5.729

Ghiorso, M. S., & Sack, R. O. (1995). Chemical mass transfer in magmatic processes IV. A revised and internally consistent thermodynamic model for the interpolation and extrapolation of liquid-solid equilibria in magmatic systems at elevated temperatures and pressures. Contributions to Mineralogy and Petrology, 119(2-3), 197-212. https://doi.org/10.1007/BF00307281

Ghiorso, M. S., Hirschmann, M. M., Reiners, P. W., & Kress, V. C. (2002). The pMELTS□: A revision of MELTS for improved calculation of phase relations and major element partitioning related to partial melting of the mantle to 3 GPa: pMELTS, A REVISION OF MELTS. *Geochemistry, Geophysics, Geosystems*, *3*(5), 1-35. https://doi.org/10.1029/2001GC000217

Godard, M., Bodinier, J.-L., & Vasseur, G. (1995). Effects of mineralogical reactions on trace element redistributions in mantle rocks during percolation processes□: A chromatographic approach. Earth and Planetary Science Letters, 133(3-4), 449-461. https://doi.org/10.1016/0012-821X(95)00104-K

Godard, M., Jousselin, D., & Bodinier, J.-L. (2000). Relationships between geochemistry and structure beneath a palaeo-spreading centre□: A study of the mantle section in the Oman ophiolite. Earth and Planetary Science Letters, 180(1-2), 133-148. https://doi.org/10.1016/S0012-821X(00)00149-7

Griffin, W. L., O'Reilly, S. Y., Afonso, J. C., & Begg, G. C. (2009). The Composition and Evolution of Lithospheric Mantle□: A Re-evaluation and its Tectonic Implications. Journal of Petrology, 50(7), 1185-1204. https://doi.org/10.1093/petrology/egn033

Griffin, W. L., O'Reilly, S. Y., & Ryan, C. G. (1999). The composition and origin of sub-continental lithospheric mantle. In Mantle Petrology□: Field Observations and High Pressure Experimentation□: A Tribute to Francis R. (Joe) Boyd (Vol. 6, p. 13-45). Geochem. Soc. Spec. Publ.

Gu, X., Deloule, E., France, L., & Ingrin, J. (2016). Multi-stage metasomatism revealed by trace element and Li isotope distributions in minerals of peridotite xenoliths from Allègre volcano (French Massif Central). Lithos, 264, 158-174. https://doi.org/10.1016/j.lithos.2016.07.019

Gu, X., Ingrin, J., Deloule, E., France, L., & Xia, Q. (2018). Metasomatism in the sub-continental lithospheric mantle beneath the south French Massif Central□: Constraints from trace elements, Li and H in peridotite minerals. *Chemical Geology*, *478*, 2-17. https://doi.org/10.1016/j.chemgeo.2017.08.006

Handler, M. R., Wysoczanski, R. J., & Gamble, J. A. (2003). Proterozoic lithosphere in Marie Byrd Land, West Antarctica□: Re–Os systematics of spinel peridotite xenoliths. Chemical Geology, 196(1-4), 131-145. https://doi.org/10.1016/S0009-2541(02)00410-2

Hellebrand, E. (2002). Garnet-field Melting and Late-stage Refertilization in « Residual » Abyssal Peridotites from the Central Indian Ridge. Journal of Petrology, 43(12), 2305-2338. https://doi.org/10.1093/petrology/43.12.2305

Hellebrand, E., Snow, J. E., Dick, H. J. B., & Hofmann, A. W. (2001). Coupled major and trace elements as indicators of the extent of melting in mid-ocean-ridge peridotites. Nature, 410(6829), 677-681. https://doi.org/10.1038/35070546

Herzberg, C. (2011). Identification of Source Lithology in the Hawaiian and Canary Islands□: Implications for Origins. Journal of Petrology, 52(1), 113-146. https://doi.org/10.1093/petrology/egq075

Herzberg, C. (2004). Geodynamic information in peridotite petrology. Journal of Petrology, 45(12), 2507-2530.

Hirose, K., & Kushiro, I. (1993). Partial melting of dry peridotites at high pressures□: Determination of compositions of melts segregated from peridotite using aggregates of diamond. Earth and Planetary Science Letters, 114(4), 477-489. https://doi.org/10.1016/0012-821X(93)90077-M

Hirschmann, M. M. (2000). Mantle solidus□: Experimental constraints and the effects of peridotite composition: MANTLE SOLIDUS. Geochemistry, Geophysics, Geosystems, 1(10), n/a-n/a. https://doi.org/10.1029/2000GC000070

Hirschmann, M. M., Ghiorso, M. S., Wasylenki, L. E., Asimow, P. D., & Stolper, E. M. (1998). Calculation of Peridotite Partial Melting from Thermodynamic Models of Minerals and Melts. I. Review of Methods and Comparison with Experiments. Journal of Petrology, 39(6), 1091-1115. https://doi.org/10.1093/petroj/39.6.1091

Hofmann, A. W. (1997). Mantle geochemistry□: The message from oceanic volcanism. Nature, 385(6613), 219-229. https://doi.org/10.1038/385219a0

Jakobsson, S. P., Jonsson, J., & Shido, F. (1978). Petrology of the Western Reykjanes Peninsula, Iceland. Journal of Petrology, 19(4), 669-705. https://doi.org/10.1093/petrology/19.4.669

Jollands, M. C., Hanger, B. J., Yaxley, G. M., Hermann, J., & Kilburn, M. R. (2018). Timescales between mantle metasomatism and kimberlite ascent indicated by diffusion profiles in garnet crystals from peridotite xenoliths. *Earth and Planetary Science Letters*, *481*, 143-153.

Kelemen, Peter. B. (1990). Reaction Between Ultramafic Rock and Fractionating Basaltic Magma I. Phase Relations, the Origin of Calc-alkaline Magma Series, and the Formation of Discordant Dunite. Journal of Petrology, 31(1), 51-98. https://doi.org/10.1093/petrology/31.1.51

Kelemen, P.B., Dick, H.J., Quick, J.E., 1992. Formation of harzburgite by pervasivemelt/rock reaction in the upper mantle. Nature 358, 635–641.

Keller, T., & Katz, R. F. (2016). The role of volatiles in reactive melt transport in the asthenosphere. Journal of Petrology, 57(6), 1073-1108.

Kornprobst, J. (1969). Le massif ultrabasique des Beni Bouchera (Rif Interne, Maroc)□: Etude des péridotites de haute température et de haute pression, et des pyroxénolites, à grenat ou sans grenat, qui leur sont associées. *Contributions to Mineralogy and Petrology*, *23*(4), 283-322. https://doi.org/10.1007/BF00371425

Kornprobst, J., Piboule, M., Roden, M., Tabit, A. (1990). Corundum-bearing garnet clinopyroxenites at Beni Bousera (Morocco): Original plagioclase-rich gabbros recrystallized at depth within the mantle? *Journal of Petrology,* 31(3), 717-745.

Kress, V. C., & Carmichael, I. S. (1988). Stoichiometry of the iron oxidation reaction in silicate melts. American Mineralogist, 73(11-12), 1267-1274.

Lambart, S., Laporte, D., & Schiano, P. (2009). An experimental study of focused magma transport and basalt–peridotite interactions beneath mid-ocean ridges□: Implications for the generation of primitive MORB compositions. *Contributions to Mineralogy and Petrology*, *157*(4), 429-451. https://doi.org/10.1007/s00410-008-0344-7

Lambart, S., Laporte, D., Provost, A., & Schiano, P. (2012). Fate of Pyroxenite-derived Melts in the Peridotitic Mantle□: Thermodynamic and Experimental Constraints. Journal of Petrology, 53(3), 451-476. https://doi.org/10.1093/petrology/egr068

Lambart, S., Laporte, D., & Schiano, P. (2013). Markers of the pyroxenite contribution in the major-element compositions of oceanic basalts□: Review of the experimental constraints. Lithos, 160-161, 14-36. https://doi.org/10.1016/j.lithos.2012.11.018

Lambart, S., Hamilton, S., & Lang, O. I. (2022). Compositional variability of San Carlos olivine. *Chemical Geology*, *605*, 120968. https://doi.org/10.1016/j.chemgeo.2022.120968

Laumonier, M., Farla, R., Frost, D. J., Katsura, T., Marquardt, K., Bouvier, A.-S., & Baumgartner, L. P. (2017). Experimental determination of melt interconnectivity and electrical conductivity in the upper mantle. Earth and Planetary Science Letters, 463, 286-297. https://doi.org/10.1016/j.epsl.2017.01.037

Lawley, C. J. M., Pearson, D. G., Waterton, P., Zagorevski, A., Bédard, J. H., Jackson, S. E., Petts, D. C., Kjarsgaard, B. A., Zhang, S., & Wright, D. (2020). Element and isotopic signature of re-fertilized mantle peridotite as determined by nanopowder and olivine LA-ICPMS analyses. Chemical Geology, 536, 119464. https://doi.org/10.1016/j.chemgeo.2020.119464

Le Roux, V., Bodinier, J.-L., Alard, O., O'Reilly, S. Y., & Griffin, W. L. (2009). Isotopic decoupling during porous melt flow□: A case-study in the Lherz peridotite. Earth and Planetary Science Letters, 279(1-2), 76-85. https://doi.org/10.1016/j.epsl.2008.12.033

Le Roux, V., Bodinier, J.-L., Tommasi, A., Alard, O., Dautria, J.-M., Vauchez, A., & Riches, A. J. V. (2007). The Lherz spinel lherzolite□: Refertilized rather than pristine mantle. Earth and Planetary Science Letters, 259(3-4), 599-612. https://doi.org/10.1016/j.epsl.2007.05.026

Le Roux, V., Nielsen, S. G., Sun, C., & Yao, L. (2016). Dating layered websterite formation in the lithospheric mantle. Earth and Planetary Science Letters, 454, 103-112. https://doi.org/10.1016/j.epsl.2016.08.036

764 Le Roux, V., Tommasi, A., & Vauchez, A. (2008). Feedback between melt percolation and deformation in an exhumed
765 lithosphere–asthenosphere boundary. Earth and Planetary Science Letters, 274(3-4), 401-413.
766 https://doi.org/10.1016/j.epsl.2008.07.053

767 Lorand, J.-P., & Luguet, A. (2016). Chalcophile and Siderophile Elements in Mantle Rocks□: Trace Elements Controlled By
768 Trace Minerals. Reviews in Mineralogy and Geochemistry, 81(1), 441-488. https://doi.org/10.2138/rmg.2016.81.08

769 Mallik, A., & Dasgupta, R. (2013). Reactive Infiltration of MORB-Eclogite-Derived Carbonated Silicate Melt into Fertile
770 Peridotite at 3 GPa and Genesis of Alkalic Magmas. Journal of Petrology, 54(11), 2267-2300.
771 https://doi.org/10.1093/petrology/egt047

772 Mallmann, G., O'Neill, H. S. C., & Klemme, S. (2009). Heterogeneous distribution of phosphorus in olivine from otherwise
773 well-equilibrated spinel peridotite xenoliths and its implications for the mantle geochemistry of lithium. *Contributions to*
774 *Mineralogy and Petrology*, *158*(4), 485-504.

775 McDonough, W. F., & Frey, F. A. (1989). Chapter 5. RARE EARTH ELEMENTS IN UPPER MANTLE ROCKS. In B. R.
776 Lipin & G. A. McKay (Éds.), Geochemistry and Mineralogy of Rare Earth Elements (p. 99-146). De Gruyter.
777 https://doi.org/10.1515/9781501509032-008

778 McKenzie, D., & Bickle, M. J. (1988). The Volume and Composition of Melt Generated by Extension of the Lithosphere.
779 Journal of Petrology, 29(3), 625-679. https://doi.org/10.1093/petrology/29.3.625

780 McKenzie, D., & O'Nions, R. K. (1991). Partial Melt Distributions from Inversion of Rare Earth Element Concentrations.
781 Journal of Petrology, 32(5), 1021-1091. https://doi.org/10.1093/petrology/32.5.1021

782 Menzies, M. A., & Dupuy, C. (1991). Orogenic Massifs□: Protolith, Process and Provenance. *Journal of Petrology*,
783 *Special_Volume*(2), 1-16. https://doi.org/10.1093/petrology/Special_Volume.2.1

784 Mitchell, A. L., & Grove, T. L. (2016). Experiments on melt–rock reaction in the shallow mantle wedge. Contributions to
785 Mineralogy and Petrology, 171(12), 107. https://doi.org/10.1007/s00410-016-1312-2

786 Morgan, Z., & Liang, Y. (2003). An experimental and numerical study of the kinetics of harzburgite reactive dissolution
787 with applications to dunite dike formation. Earth and Planetary Science Letters, 214(1-2), 59-74.
788 https://doi.org/10.1016/S0012-821X(03)00375-3

789 Morgan, Z., & Liang, Y. (2005). An experimental study of the kinetics of lherzolite reactive dissolution with applications to
790 melt channel formation. *Contributions to Mineralogy and Petrology*, *150*(4), 369-385. https://doi.org/10.1007/s00410-005-
791 0033-8

Mundl, A., Ntaflos, T., Ackerman, L., Bizimis, M., Bjerg, E. A., Wegner, W., & Hauzenberger, C. A. (2016). Geochemical and Os–Hf–Nd–Sr Isotopic Characterization of North Patagonian Mantle Xenoliths□: Implications for Extensive Melt Extraction and Percolation Processes. Journal of Petrology, 57(4), 685-715. https://doi.org/10.1093/petrology/egv048

Müntener, O., Pettke, T., Desmurs, L., Meier, M., & Schaltegger, U. (2004). Refertilization of mantle peridotite in embryonic ocean basins□: Trace element and Nd isotopic evidence and implications for crust–mantle relationships. Earth and Planetary Science Letters, 221(1-4), 293-308. https://doi.org/10.1016/S0012-821X(04)00073-1

Müntener, O., & Piccardo, G. B. (2003). Melt migration in ophiolitic peridotites□: The message from Alpine-Apennine peridotites and implications for embryonic ocean basins. Geological Society, London, Special Publications, 218(1), 69-89. https://doi.org/10.1144/GSL.SP.2003.218.01.05

Navon, O., & Stolper, E. (1987). Geochemical Consequences of Melt Percolation□: The Upper Mantle as a Chromatographic Column. The Journal of Geology, 95(3), 285-307. https://doi.org/10.1086/629131

Norman, M. D., & Garcia, M. O. (1999). Primitive magmas and source characteristics of the Hawaiian plume□: Petrology and geochemistry of shield picrites. Earth and Planetary Science Letters, 168(1-2), 27-44. https://doi.org/10.1016/S0012-821X(99)00043-6

Niu, Y. (1997). Mantle Melting and Melt Extraction Processes beneath Ocean Ridges□: Evidence from Abyssal Peridotites. Journal of Petrology, 38(8), 1047-1074. https://doi.org/10.1093/petroj/38.8.1047

O'Driscoll, B., Walker, R. J., Day, J. M. D., Ash, R. D., & Daly, J. S. (2015). Generations of Melt Extraction, Melt–Rock Interaction and High-Temperature Metasomatism Preserved in Peridotites of the ~497 Ma Leka Ophiolite Complex, Norway. Journal of Petrology, 56(9), 1797-1828. https://doi.org/10.1093/petrology/egv055

Oliveira, B., Afonso, J. C., & Tilhac, R. (2020). A disequilibrium reactive transport model for mantle magmatism. Journal of Petrology, 61(9), egaa067.

Pearson, D. G., Canil, D., & Shirey, S. B. (2014). Mantle Samples Included in Volcanic Rocks. In Treatise on Geochemistry (p. 169-253). Elsevier. https://doi.org/10.1016/B978-0-08-095975-7.00216-3

Pec, M., Holtzman, B. K., Zimmerman, M., & Kohlstedt, D. L. (2015). Reaction infiltration instabilities in experiments on partially molten mantle rocks. Geology, 43(7), 575-578.

Pilet, S., Baker, M. B., Müntener, O., & Stolper, E. M. (2011a). Monte Carlo Simulations of Metasomatic Enrichment in the Lithosphere and Implications for the Source of Alkaline Basalts. Journal of Petrology, 52(7-8), 1415-1442. https://doi.org/10.1093/petrology/egr007

Pilet, S., Baker, M. B., Müntener, O., & Stolper, E. M. (2011b). Monte Carlo Simulations of Metasomatic Enrichment in the Lithosphere and Implications for the Source of Alkaline Basalts. Journal of Petrology, 52(7-8), 1415-1442. https://doi.org/10.1093/petrology/egr007

Pilet, S., Baker, M. B., & Stolper, E. M. (2008). Metasomatized Lithosphere and the Origin of Alkaline Lavas. Science, 320(5878), 916-919. https://doi.org/10.1126/science.1156563

Pilet, S., Hernandez, J., Sylvester, P., & Poujol, M. (2005). The metasomatic alternative for ocean island basalt chemical heterogeneity. Earth and Planetary Science Letters, 236(1-2), 148-166. https://doi.org/10.1016/j.epsl.2005.05.004

Raffone, N., Chazot, G., Pin, C., Vannucci, R., & Zanetti, A. (2009). Metasomatism in the Lithospheric Mantle beneath Middle Atlas (Morocco) and the Origin of Fe- and Mg-rich Wehrlites. Journal of Petrology, 50(2), 197□249. https://doi.org/10.1093/petrology/egn069

Rampone, E., Borghini, G., & Basch, V. (2020). Melt migration and melt-rock reaction in the Alpine-Apennine peridotites□: Insights on mantle dynamics in extending lithosphere. Geoscience Frontiers, 11(1), 151-166. https://doi.org/10.1016/j.gsf.2018.11.001

Reisberg, L. (2021). Osmium isotope constraints on formation and refertilization of the non-cratonic continental mantle lithosphere. Chemical Geology, 574, 120245. https://doi.org/10.1016/j.chemgeo.2021.120245

Rudnick, R. L., & Walker, R. J. (2009). Interpreting ages from Re–Os isotopes in peridotites. Lithos, 112, 1083-1095. https://doi.org/10.1016/j.lithos.2009.04.042

Saal, A. E. (2001). Re-Os Isotopes in the Horoman Peridotite□: Evidence for Refertilization? Journal of Petrology, 42(1), 25-37. https://doi.org/10.1093/petrology/42.1.25

Seyler, M., Lorand, J.-P., Dick, H. J. B., & Drouin, M. (2007). Pervasive melt percolation reactions in ultra-depleted refractory harzburgites at the Mid-Atlantic Ridge, 15° 20′N□: ODP Hole 1274A. Contributions to Mineralogy and Petrology, 153(3), 303-319. https://doi.org/10.1007/s00410-006-0148-6

Shaw, C. S. J., Lebert, B. S., & Woodland, A. B. (2018). Thermodynamic Modelling of Mantle–Melt Interaction Evidenced by Veined Wehrlite Xenoliths from the Rockeskyllerkopf Volcanic Complex, West Eifel Volcanic Field, Germany. Journal of Petrology, 59(1), 59-86. https://doi.org/10.1093/petrology/egy018

Simon, N. S. C., Carlson, R. W., Pearson, D. G., & Davies, G. R. (2007). The Origin and Evolution of the Kaapvaal Cratonic Lithospheric Mantle. Journal of Petrology, 48(3), 589-625. https://doi.org/10.1093/petrology/egl074

847 Simon, N. S. C., Neumann, E.-R., Bonadiman, C., Coltorti, M., Delpech, G., Grégoire, M., & Widom, E. (2008). Ultra-
848 refractory Domains in the Oceanic Mantle Lithosphere Sampled as Mantle Xenoliths at Ocean Islands. Journal of Petrology,
849 49(6), 1223-1251. https://doi.org/10.1093/petrology/egn023

850 Smith, P. M., & Asimow, P. D. (2005). Adiabat_1ph□: A new public front-end to the MELTS, pMELTS, and pHMELTS
851 models: ADIABAT_1PH FRONT-END. Geochemistry, Geophysics, Geosystems, 6(2).
852 https://doi.org/10.1029/2004GC000816

853 Sobolev, A. V., Hofmann, A. W., Sobolev, S. V., & Nikogosian, I. K. (2005). An olivine-free mantle source of Hawaiian
854 shield basalts. Nature, 434(7033), 590-597. https://doi.org/10.1038/nature03411

855 Song, Y., & Frey, F. A. (1989). Geochemistry of peridotite xenoliths in basalt from Hannuoba, Eastern China□: Implications
856 for subcontinental mantle heterogeneity. Geochimica et Cosmochimica Acta, 53(1), 97-113. https://doi.org/10.1016/0016-
857 7037(89)90276-7

858 Soustelle, V., Tommasi, A., Bodinier, J. L., Garrido, C. J., & Vauchez, A. (2009). Deformation and Reactive Melt Transport
859 in the Mantle Lithosphere above a Large-scale Partial Melting Domain□: The Ronda Peridotite Massif, Southern Spain.
860 Journal of Petrology, 50(7), 1235-1266. https://doi.org/10.1093/petrology/egp032

861 Soustelle, V., Walte, N. P., Manthilake, M. A. G. M., & Frost, D. J. (2014). Melt migration and melt-rock reactions in the
862 deforming Earth's upper mantle□: Experiments at high pressure and temperature. Geology, 42(1), 83-86.
863 https://doi.org/10.1130/G34889.1

864 Stolper, E. (1980). A phase diagram for mid-ocean ridge basalts: preliminary results and implications for petrogenesis.
865 Contributions to Mineralogy and Petrology, 74(1), 13-27. doi:10.1007/BF00375485

866 Stracke, A., Hofmann, A. W., & Hart, S. R. (2005). FOZO, HIMU, and the rest of the mantle zoo□: THE MANTLE ZOO.
867 Geochemistry, Geophysics, Geosystems, 6(5), n/a-n/a. https://doi.org/10.1029/2004GC000824

868 Tilhac, R., Morishita, T., Hanaue, N., Tamura, A., & Guotana, J. M. (2021). Systematic LREE enrichment of mantle
869 harzburgites: The petrogenesis of San Carlos xenoliths revisited. Lithos, 396, 106195.

870 Tilhac, R., Ceuleneer, G., Griffin, W. L., O'Reilly, S. Y., Pearson, N. J., Benoit, M., ... & Grégoire, M. (2016). Primitive arc
871 magmatism and delamination: petrology and geochemistry of pyroxenites from the Cabo Ortegal Complex, Spain. Journal of
872 Petrology, 57(10), 1921-1954.

873 Tomlinson, E. L., & Kamber, B. S. (2021). Depth-dependent peridotite-melt interaction and the origin of variable silica in
874 the cratonic mantle. Nature Communications, 12(1), 1082. https://doi.org/10.1038/s41467-021-21343-9

875 Turner, A. J., Katz, R. F., & Behn, M. D. (2015). Grain□size dynamics beneath mid□ocean ridges: Implications for
876 permeability and melt extraction. Geochemistry, Geophysics, Geosystems, 16(3), 925-946.

877 Van der Wal, D. V., & Bodinier, J.-L. (1996). Origin of the recrystallisation front in the Ronda peridotite by km-scale
878 pervasive porous melt flow. Contributions to Mineralogy and Petrology, 122(4), 387-405.
879 https://doi.org/10.1007/s004100050135

880 Waff, H. S., & Faul, U. H. (1992). Effects of crystalline anisotropy on fluid distribution in ultramafic partial melts. Journal
881 of Geophysical Research, 97(B6), 9003. https://doi.org/10.1029/92JB00066

882 Wang, C., Liang, Y., Dygert, N., & Xu, W. (2016). Formation of orthopyroxenite by reaction between peridotite and
883 hydrous basaltic melt: an experimental study. Contributions to Mineralogy and Petrology, 171(8), 1-18.

884 Warren, J. M. (2016). Global variations in abyssal peridotite compositions. Lithos, 248-251, 193-219.
885 https://doi.org/10.1016/j.lithos.2015.12.023

886 Watson, E. B., Brenan, J. M., Baker, D. R. (1990). "Distribution of fluids in the continental mantle." In Continental mantle,
887 Oxford Clarendon Press, pp. 111-125. 1990.

888 Wu, F.-Y., Walker, R. J., Yang, Y.-H., Yuan, H.-L., & Yang, J.-H. (2006). The chemical-temporal evolution of lithospheric
889 mantle underlying the North China Craton. Geochimica et Cosmochimica Acta, 70(19), 5013-5034.
890 https://doi.org/10.1016/j.gca.2006.07.014

891 Yaxley, G. M., & Green, D. H. (1998). Reactions between eclogite and peridotite□: Mantle refertilisation by subduction of
892 oceanic crust. Schweizerische mineralogische und petrographische Mitteilungen, 78(2), 243-255.

893 Zhu, W., Gaetani, G. A., Fusseis, F., Montesi, L. G. J., & De Carlo, F. (2011). Microtomography of Partially Molten
894 Rocks□: Three-Dimensional Melt Distribution in Mantle Peridotite. Science, 332(6025), 88-91.
895 https://doi.org/10.1126/science.1202221

896

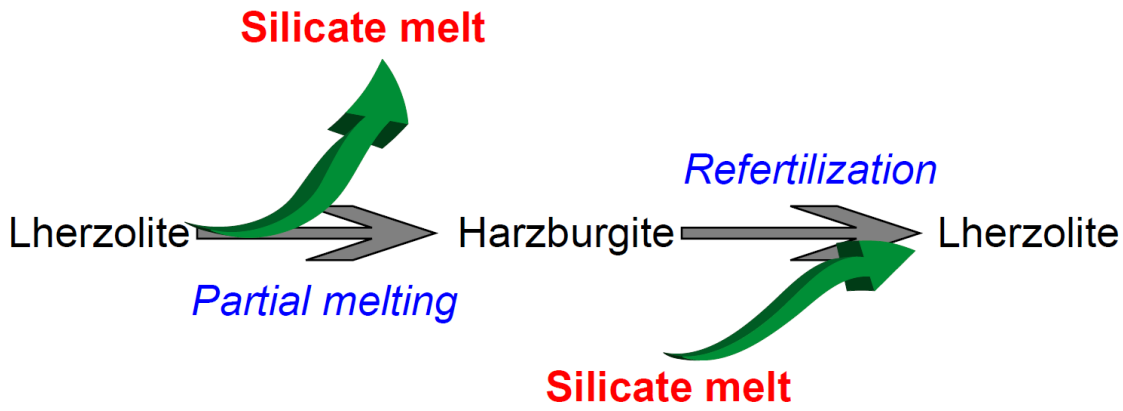

897
898 *Fig 1. Schematization of the refertilization process in the context of lithospheric dynamics.*

899

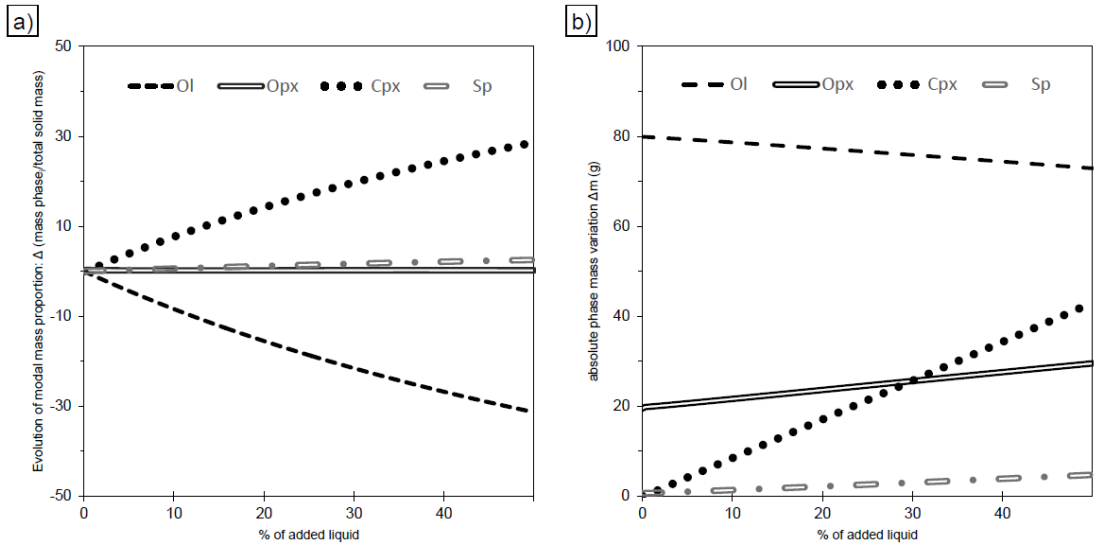

900

901 *Fig 2. Evolution of modal mass proportions (in wt.%) of the different phases as a function of % of*
902 *liquid added for run #1. a) Difference between modal proportion of each phase in the impregnated*
903 *peridotite and its initial modal proportion in the starting material. For example, olivine represents*
904 *79.9 wt.% of the initial starting material but only 48.6 wt.% of the solid phase present at the end of*
905 *the experiment, a change of -31.3. b) Absolute mass variation of each phase, for olivine, 79.9g of*
906 *material are present at the beginning of the run, but only 72.9g at the end. (Ol: Olivine; Opx:*
907 *Orthopyroxene; Cpx: Clinopyroxene; Sp: Spinel)*

908

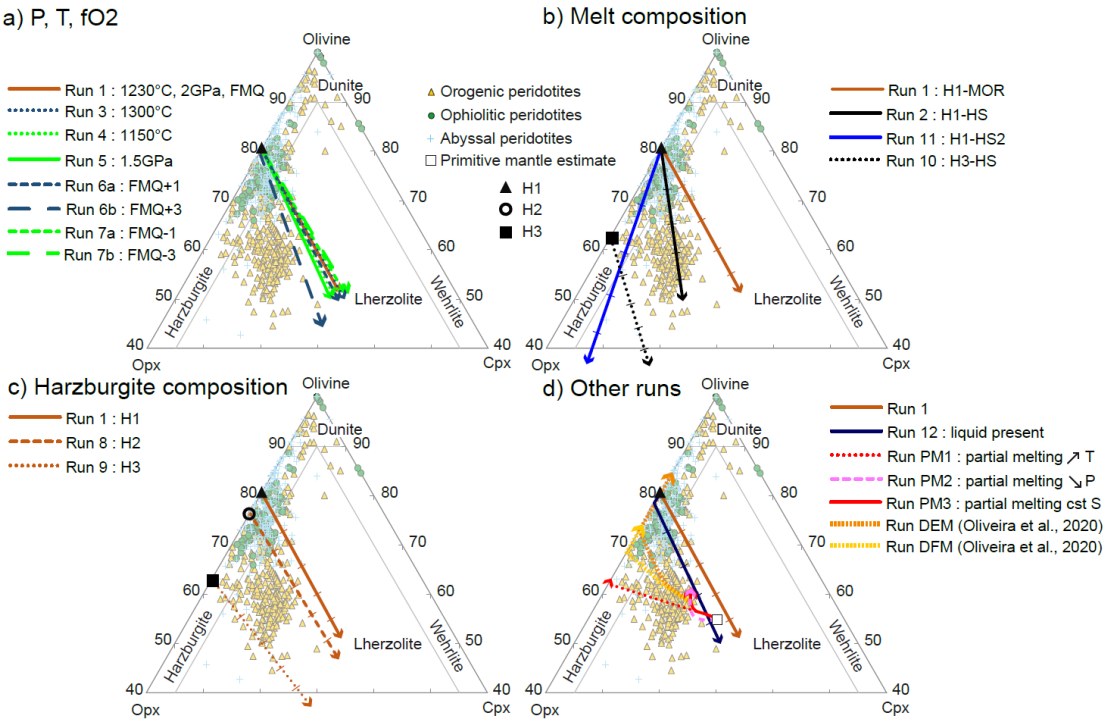

Fig 3. Evolution of modal proportions in models. Arrows indicate the direction of evolution of each run. In the impregnation calculations (runs #1 to #11), each tick mark indicates an addition of 10% of liquid. a) Runs #1 to #7b: influence of variations in pressure, temperature and redox conditions. b) Runs #1, #2, #10, and #11: influence of the chemical composition of the percolating melt c) Runs #1, #8, and #9: influence of the chemical composition of percolated harzburgite. d) Run #12: liquid-phase present run; run PM1: partial melting by isobaric rising temperature; run PM2: partial melting by decompression at constant T; run PM3: partial melting by isentropic decompression (constant S); and run #1: reference run. Partial melting runs by Oliveira et al., 2020 are shown for comparison (DEM: Dynamic Equilibrium Melting; DFM: Dynamic Fractional Melting). Primitive upper mantle estimate is from McDonough, 1995. Results are compared with modal proportions of a global database of tectonically emplaced peridotites (Bodinier & Godard, 2014, and references therein).

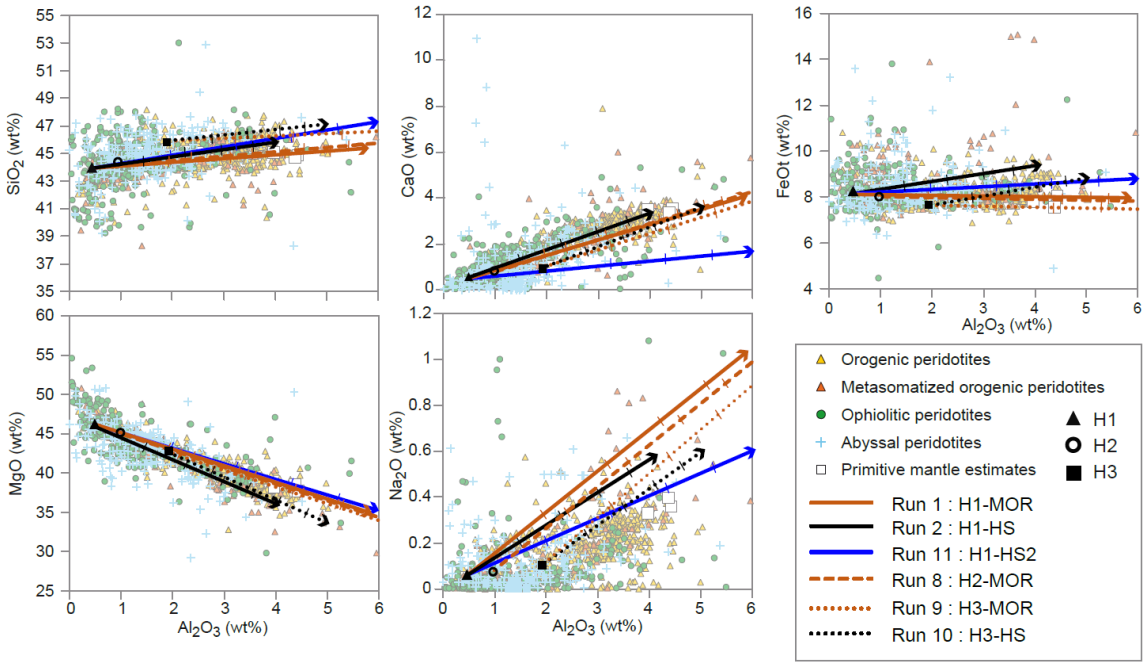

922

923 *Fig 4. Chemical diagrams displaying the variation of major element oxides (wt%) of the 6 runs*
924 *comparing the influence of compositional variations (runs #1, #8, and #9: variation of the harzburgite*
925 *composition; runs #1, #2, #10, and #11: variation of the percolating melt composition). Arrows*
926 *indicate the direction of evolution of each test. Crosses on slopes are every 10% of liquid added.*
927 *FeO_t: total iron content expressed as FeO. Results are compared with a global database of peridotites*
928 *(Bodinier & Godard, 2014, and references therein).*

929

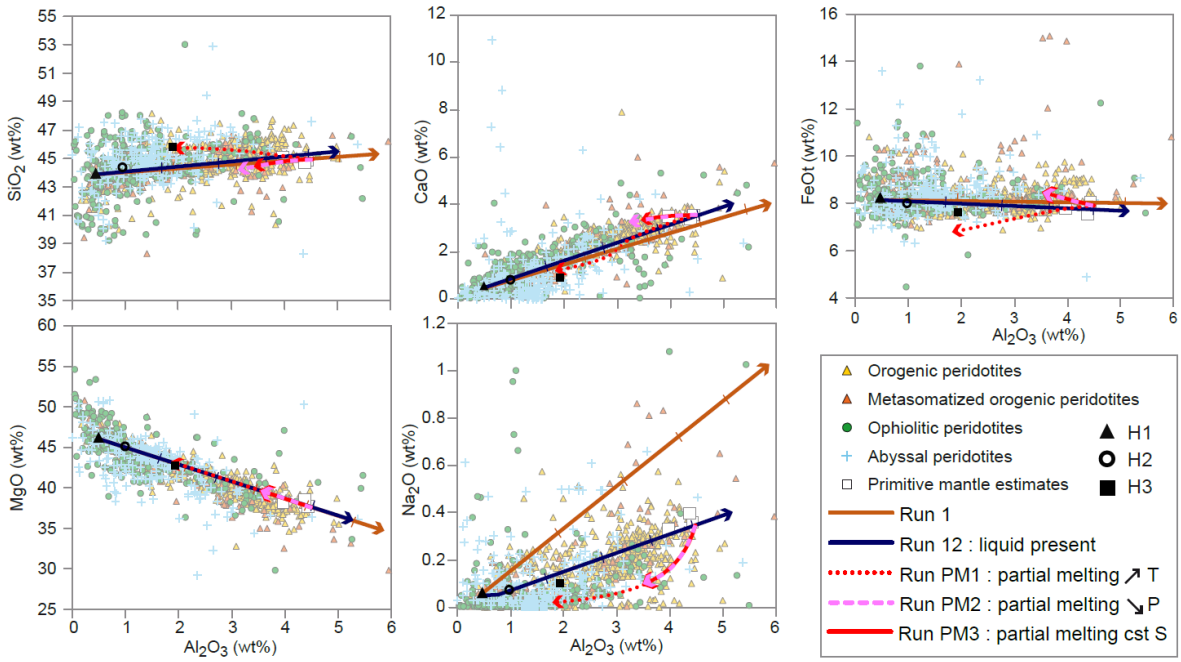

930

931 *Fig 5. Variation of bulk major element concentrations (wt%) for the residual solid phase in runs #1,*
932 *#12, PM1, PM2 and PM3. Run #12 is an impregnation run performed with a liquid phase present.*
933 *Run PM1 is an isobaric partial melting run. Run PM2 is a partial melting run by decompression at*
934 *constant T. Run PM3 is a partial melting run by isentropic decompression. Run #1 is shown for*
935 *comparison. Arrows indicate the direction of evolution of each test. For runs #12 and #1, tick-marks*
936 *on arrows indicate every 10% of liquid added. FeO_t: total iron content expressed as FeO. Results are*
937 *compared with a global database of peridotites (Bodinier & Godard, 2014, and references therein).*

938

Table 1. Summary of thermodynamic parameters used in the calculations: temperature (T), pressure (P), oxygen fugacity (fO_2), starting composition and basaltic melt composition. (PM: Partial Melting; FMQ: Fayalite-Magnetite-Quartz oxygen buffer; H: Harzburgite; PUM: Primitive Upper Mantle; MOR: Mid-Ocean Ridge; HS: Hot Spot)

Run n°	T (°C)	P (GPa)	fO_2	Starting composition	Melt composition
1	1230	2	FMQ	H1	MOR
2	1230	2	FMQ	H1	HS
3[a]	1300	2	FMQ	H1	MOR
4	1150	2	FMQ	H1	MOR
5[a]	1230	1.5	FMQ	H1	MOR
6a	1230	2	FMQ+1	H1	MOR
6b	1230	2	FMQ+3	H1	MOR
7a	1230	2	FMQ-1	H1	MOR
7b	1230	2	FMQ-3	H1	MOR
8	1230	2	FMQ	H2	MOR
9	1230	2	FMQ	H3	MOR
10	1230	2	FMQ	H3	HS
11	1230	2	FMQ	H1	HS2
12[a]	1400	2	FMQ	H1	MOR
PM1	1200 - 1520	2	FMQ	PUM	-
PM2[b]	1230	2 – 0.6	FMQ	PUM	-
PM3[c]	1396 - 1213	2 – 0.6	FMQ	PUM	-

[a] Liquid-present runs
[b] Isothermal run
[c] Isentropic run

Table 2. Chemical compositions of peridotites used in calculations.[a] (H: Harzburgite; PUM: Primitive Upper Mantle)

	SiO_2	Al_2O_3	FeOt	MnO	MgO	CaO	Na_2O	Cr_2O_3	TiO_2
H1[b]	43.91	0.47	8.19	0.13	46.57	0.38	0.05	0.31	0.01
H2[b]	44.34	0.97	7.99	0.13	45.39	0.64	0.06	0.46	0.02
H3[b]	45.82	1.92	7.49	0.13	42.95	0.75	0.09	0.82	0.04
PUM[c]	45.03	4.45	8.06	0.14	37.83	3.55	0.36	0.38	0.20

[a] All compositions are normalized to 100 wt %. FeO_t: total iron content expressed as FeO.
[b] Le Roux et al.,2007; [c]McDonough, 1995.

Table 3. Chemical compositions of percolating basaltic melts used in calculations.[a] (MOR: Mid-Ocean Ridge; HS: Hot Spot)

	SiO_2	Al_2O_3	FeOt	MnO	MgO	CaO	Na_2O	Cr_2O_3	TiO_2	$a_{SiO2\ b}$
MOR[c]	48.76	16.65	7.20	0.14	11.48	11.75	3.03	0.12	0.87	0.372
HS[d]	50.01	11.37	11.48	0.18	13.98	9.26	1.66	0.00	2.06	0.485
HS2[e]	54.32	17.18	9.93	0.18	11.98	3.87	1.73	0.12	0.69	0.551

[a] *All compositions are normalized to 100 wt %. FeO_t: total iron content expressed as FeO.*
[b] *Silica activities were calculated using the MELTS supplemental calculator.*
[c] *Lambart et al.,, 2009;* [d] *Norman & Garcia, 1999;* [e] *Jakobsson, 1978.*

Table 4. Final phases proportions for all runs (in wt.%). (PM: Partial Melting)

Run n°	Liquid	Olivine	Orthopyroxene	Clinopyroxene	Spinel
1	0.0	48.6	19.7	28.6	3.1
2	0.0	48.7	30.2	19.5	1.5
3	0.9	47.6	19.4	28.9	3.1
4	0.0	48.6	21.2	27.0	3.3
5	1.6	47.3	21.7	26.2	3.3
6a	0.0	47.5	20.8	28.4	3.3
6b	0.0	42.5	25.8	27.4	4.4
7a	0.0	49.2	19.0	28.8	3.1
7b	0.0	49.7	18.4	28.9	3.0
8	0.0	44.7	22.3	29.3	3.7
9	0.0	35.0	31.3	29.0	4.6
10	0.0	34.6	42.4	19.8	3.1
11	0.0	35.1	52.5	8.5	3.9
12[a]	7.5	44.0	21.8	23.8	3.0
PM1	29.8	43.8	25.2	0.0	1.2
PM2[b]	7.5	56.2	20.9	12.7	2.8
PM3[c]	4.9	57.7	21.6	13.0	2.7

[a] Liquid-present run
[b] Isothermal run
[c] Isentropic run